

## Supplementary Material

### Sustainable catalytic oxidation of 1,3-butadiene over dispersedly assembled

#### $\text{Ce}_{0.027}\text{W}_{0.02}\text{Mn}_{0.054}\text{TiO}_x$ featuring the synergistic redox cycles

Qianqian Li <sup>a,b</sup>, Chuanqi Li <sup>a,b</sup>, Mengjing Wang <sup>c</sup>, Guijin Su <sup>a,b\*</sup>, Bohua Sun <sup>a,b</sup>,

Mingge Wu <sup>a,b</sup>, Zhiwei Zhou <sup>a,b</sup>, Jiaxin Pang <sup>a,b</sup>, Jing Meng <sup>a,b</sup>, Bin Shi <sup>a,b</sup>

<sup>a</sup>Key Laboratory of Environmental Nanotechnology and Health Effects, State Key Laboratory of Environmental Chemistry and Ecotoxicology, Research Center for Eco-Environmental Sciences, Chinese Academy of Sciences, P.O. Box 2871, Beijing 100085, China;

<sup>b</sup>University of Chinese Academy of Sciences, Beijing 100049, China;

<sup>c</sup>State Key Laboratory of Marine Pollution, City University of Hong Kong, Kowloon, Hong Kong, China.

\*Corresponding author: Dr. Guijin Su; Tel: +86 10 62847550; Fax: + 86 10 62923563;

E-mail address: gjsu@rcees.ac.cn (G. Su).

## List of Supporting Information contents:

- **Content S1.** Catalyst preparation and characterizations.
- **Content S2.** The mechanism of catalyst construction by two-stage co-precipitation method
- **Fig. S1.** Schematic of the continuous-flow fixed-bed microreactor used in the present study.
- **Fig. S2.** The color of precipitant at different pH values and the relevant  $\text{Ce}_{0.027}\text{W}_{0.02}\text{Mn}_{0.054}\text{TiO}_x$  precursor during the preparation process using the two-step precipitation approach.
- **Fig. S3.** The bright-field TEM and the relevant HAADF images of  $\text{Ce}_{0.027}\text{W}_{0.02}\text{Mn}_{0.054}\text{TiO}_x$ .
- **Fig. S4.** The bright-field TEM and the relevant HAADF images of  $\text{Ce}_{0.027}\text{W}_{0.02}\text{Mn}_{0.054}\text{TiO}_x$ .
- **Fig. S5.** The W4f XPS of  $\text{Ce}_{0.027}\text{W}_{0.02}\text{Mn}_{0.054}\text{TiO}_x$  catalyst.
- **Fig. S6.** The O1s XPS spectrum of the used Ti-based catalysts.
- **Fig. S7.** In-situ DRIFTS spectra of 1,3-BD oxidation over  $\text{Ce}_{0.027}\text{Mn}_{0.054}\text{TiO}_x$ ,  $\text{Mn}_{0.054}\text{TiO}_x$  and  $\text{W}_{0.02}\text{Mn}_{0.054}\text{TiO}_x$  at different reaction temperature.
- **Fig. S8.** In situ DRIFT spectra of the  $\text{Ce}_{0.027}\text{W}_{0.02}\text{Mn}_{0.054}\text{TiO}_x/1,3\text{-BD}$  and  $\text{Ce}_{0.027}\text{W}_{0.02}\text{Mn}_{0.054}\text{TiO}_x/10\text{ vol.}\%$  water vapor reaction systems.
- **Table S1.** Variation in the mass proportion of Ce, W, Mn and Ti with the increase of the solution pH during the preparation of  $\text{Ce}_{0.027}\text{W}_{0.02}\text{Mn}_{0.054}\text{TiO}_x$  precursor by two-stage precipitation approach.

## Content S1. Catalyst preparation and characterizations

Appropriate amounts of  $\text{MnSO}_4 \cdot \text{H}_2\text{O}$ ,  $\text{Ce}(\text{NO}_3)_3 \cdot 6\text{H}_2\text{O}$ ,  $\text{H}_{26}\text{N}_6\text{O}_{40}\text{W}_{12}$ ,  $\text{Ti}(\text{SO}_4)_2$  and oxalate were firstly dissolved in deionized water at room temperature, then certain urea was added and stirred for 0.5 h. The mixture was heated up to 80 °C and stirred for 2 h. Hereafter ammonia solution was added slowly to the above solution under vigorous stirring until pH is 7. After keeping the pH value and temperature unchanged and continuing to stir for 3 h, the obtained precipitate was filtered and washed with deionized water five times. The resulting powder was dried at 80 °C for 12 h and then calcined in air at 500 °C for 5 h. The sample resulting from this method was labeled  $\text{Ce}_{0.027}\text{W}_{0.02}\text{Mn}_{0.054}\text{TiO}_x$ . Besides,  $\text{TiO}_2$ ,  $\text{Ce}_{0.027}\text{TiO}_x$ ,  $\text{Mn}_{0.054}\text{TiO}_x$ ,  $\text{Ce}_{0.027}\text{W}_{0.02}\text{TiO}_x$ ,  $\text{Ce}_{0.027}\text{Mn}_{0.054}\text{TiO}_x$  and  $\text{W}_{0.02}\text{Mn}_{0.054}\text{TiO}_x$  catalysts were also prepared by the above method to explore the interaction among the components.

X-ray diffraction (XRD) measurements were carried out on a PANalytical X'PertPro X-ray Diffractometer with Cu  $K\alpha$  radiation at the  $2\theta$  angle range from 5° to 90°. Scanning electronic microscopy (SEM) was taken to obtain images of samples by a Hitachi SU-8020 instrument. The elemental content of samples was characterized by using energy-dispersive X-ray spectroscopy (EDX). The morphology of prepared catalysts was characterized by a high-resolution transmission electron microscope (HRTEM, JEM-2100F, JEOL, Japan), and a high-angle annular dark-field scanning transmission electron microscopy (HAADF-STEM, JEM-ARM 200F, JEOL, Japan), operating on the Cs-corrected at 200 kV.  $\text{N}_2$  adsorption-desorption isotherms were available using a Micromeritics ASAP-2460 system and the specific surface area was

calculated by the BET (Brunauer-Emmett-Teller) equation. The H<sub>2</sub>O temperature-programmed desorption (H<sub>2</sub>O-TPD) analyses were carried out by a TPD apparatus equipped with a mass analyzer. Specifically, 50 mg samples were taken and purged with He at 150°C until the signal was stable, and then purged with H<sub>2</sub>O/He until the saturation adsorption of H<sub>2</sub>O. After being swept by pure He for 1 h at room temperature, the sample was heated from 100°C to 700°C to record the mass signal of H<sub>2</sub>O. The X-ray photoelectron spectroscopy (XPS) measurements were performed using the ESCALAB 250Xi system (ThermoFisher) with Al-Kα radiation as the excitation source. H<sub>2</sub> temperature-programmed reduction (H<sub>2</sub>-TPR) experiments were conducted on a chemisorption analyzer (Micromeritics, AutoChem II 2920 V5.00) under a 5% H<sub>2</sub> gas flow (30 mL min<sup>-1</sup>) at a rate of 10 °C min<sup>-1</sup> up to 900 °C. Raman spectra of catalysts were obtained by Laser Micro-Raman Spectrometer, and the wavelength and power were set as 532 nm and 5 mW. In-situ diffuse reflectance infrared Fourier transform (DRIFT) spectroscopy was obtained by a Bruker VERTEX 70 instrument scanning from 4000 to 500 cm<sup>-1</sup> at a resolution of 4 cm<sup>-1</sup>.

## **Content S2. The mechanism of catalyst construction by two-stage co-precipitation method**

For the two-stage precipitation approach, the variation in the mass proportion of Ce, W, Mn and Ti in precursor with the increase of the solution pH was measured by EDX, as shown in Table S1. The color of precipitant and the relevant precursor at different pH values were also exhibited in Figure S2. When urea was added as the first-stage

precipitation and stirred for 2 h, the pH of the solution was 0.8. Currently, the mass proportion of Ti species in the precursor was highest at 16.43%, while that of other metal species was negligible (Table S1). It means that the white precipitate mainly corresponds to  $\text{Ti}^{4+}$  species (Figure S2). This might be attributed to the preferential combination of  $\text{Ti}^{4+}$  with the limited amounts of  $\text{OH}^-$  species generated by the slow decomposition of urea. Then ammonia was used as the subsequent precipitant and added dropwise to the solution, gradually adjusting the pH to 7. During the above process, the mass proportion of Ti of  $\text{Ce}_{0.027}\text{W}_{0.02}\text{Mn}_{0.054}\text{TiO}_x$  precursor was constant at pH 1.5. Whereafter, W, Ce and Mn species were gradually precipitated at pH 1.5, 5 and 7, respectively. The color of the precipitate correspondingly changed, by degrees, from white to light yellow, then turned brown, and finally, dark brown with the increase of pH value (Figure S2). The addition of ammonia afforded the high concentrations of  $\text{OH}^-$  that could combine with the residual  $\text{Ti}^{4+}$  and subsequently with W, Ce and Mn species. These results indicated that the precipitation of Ti species was initially formed, and then W, Ce and Mn species precipitated in their outer layers in turn.

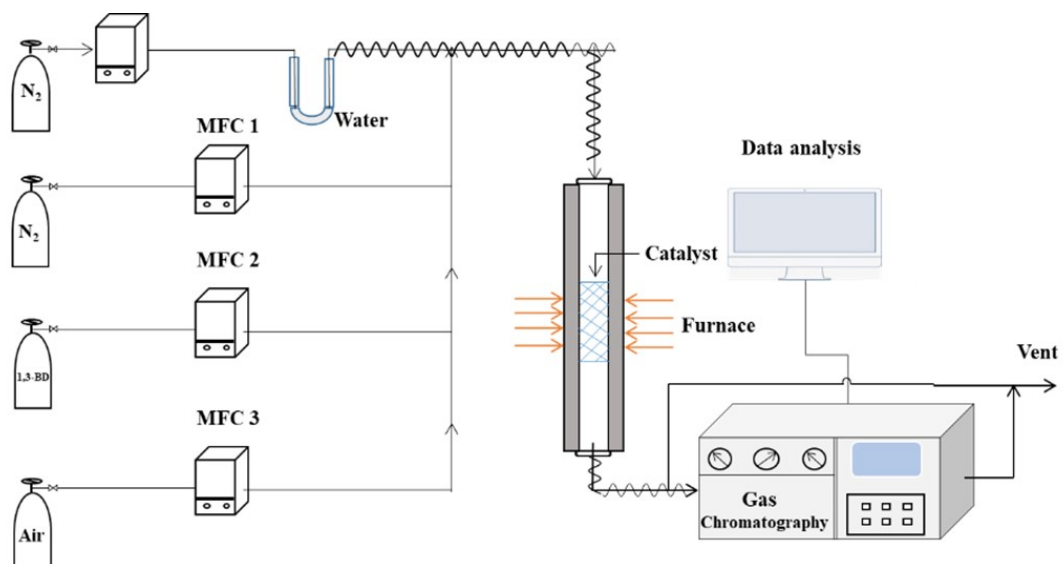


**Fig. S1.** Schematic of the continuous-flow fixed-bed microreactor used in the present study.



**Fig. S2.** The color of precipitant at different pH values and the relevant  $\text{Ce}_{0.027}\text{W}_{0.02}\text{Mn}_{0.054}\text{TiO}_x$  precursor during the preparation process using the two-step precipitation approach.

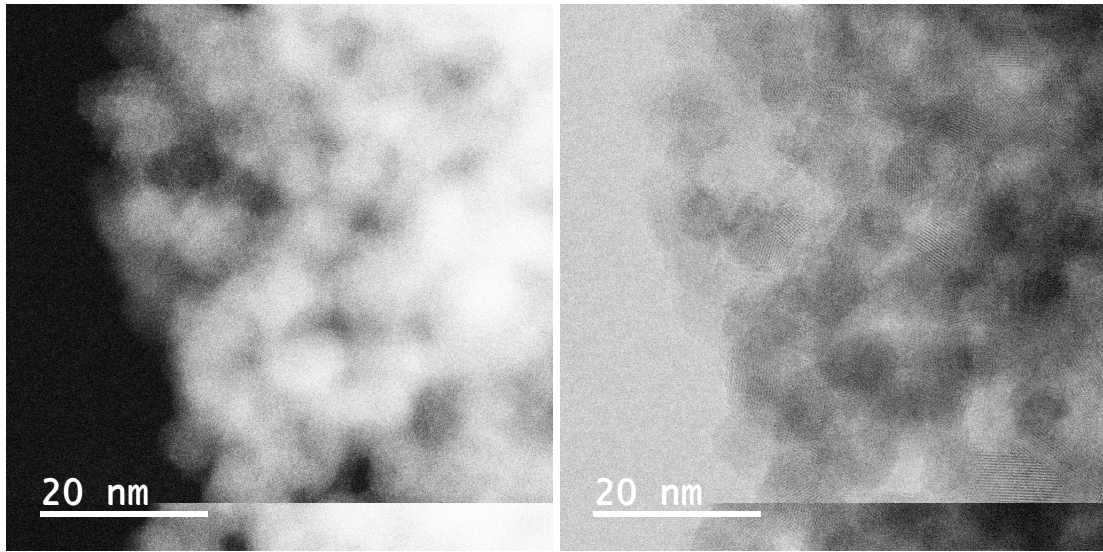


**Fig. S3.** The bright-field TEM and the relevant HAADF images of  $\text{Ce}_{0.027}\text{W}_{0.02}\text{Mn}_{0.054}\text{TiO}_x$ .

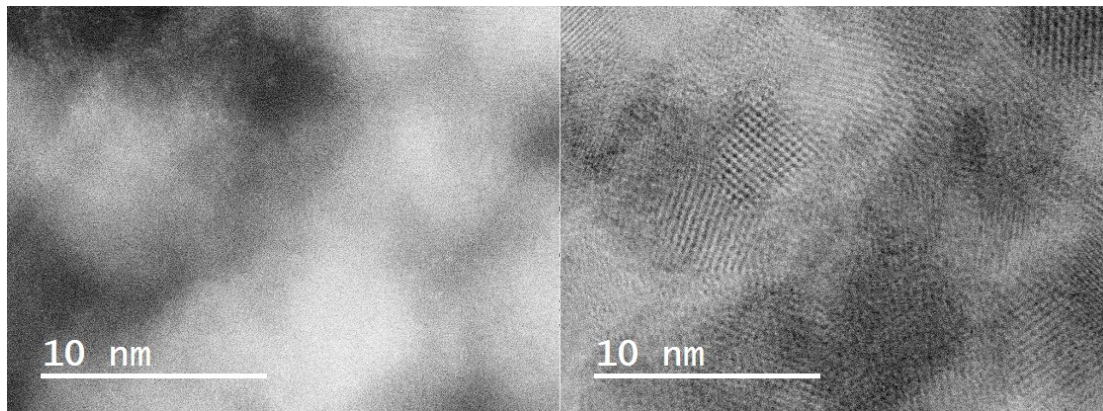


**Fig. S4.** The bright-field TEM and the relevant HAADF images of  $\text{Ce}_{0.027}\text{W}_{0.02}\text{Mn}_{0.054}\text{TiO}_x$ .

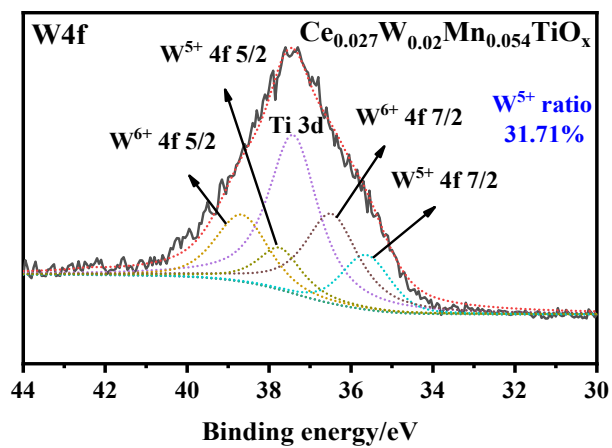


**Fig. S5.** The W4f XPS of  $\text{Ce}_{0.027}\text{W}_{0.02}\text{Mn}_{0.054}\text{TiO}_x$  catalyst.

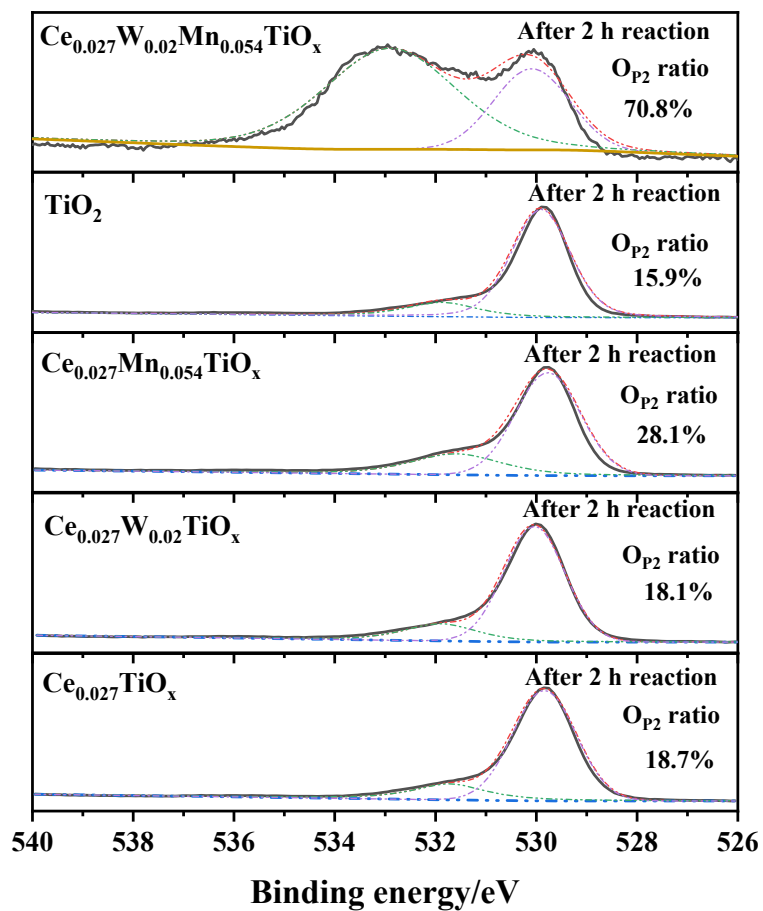


**Fig. S6.** The O1s XPS spectrum of the used Ti-based catalysts.

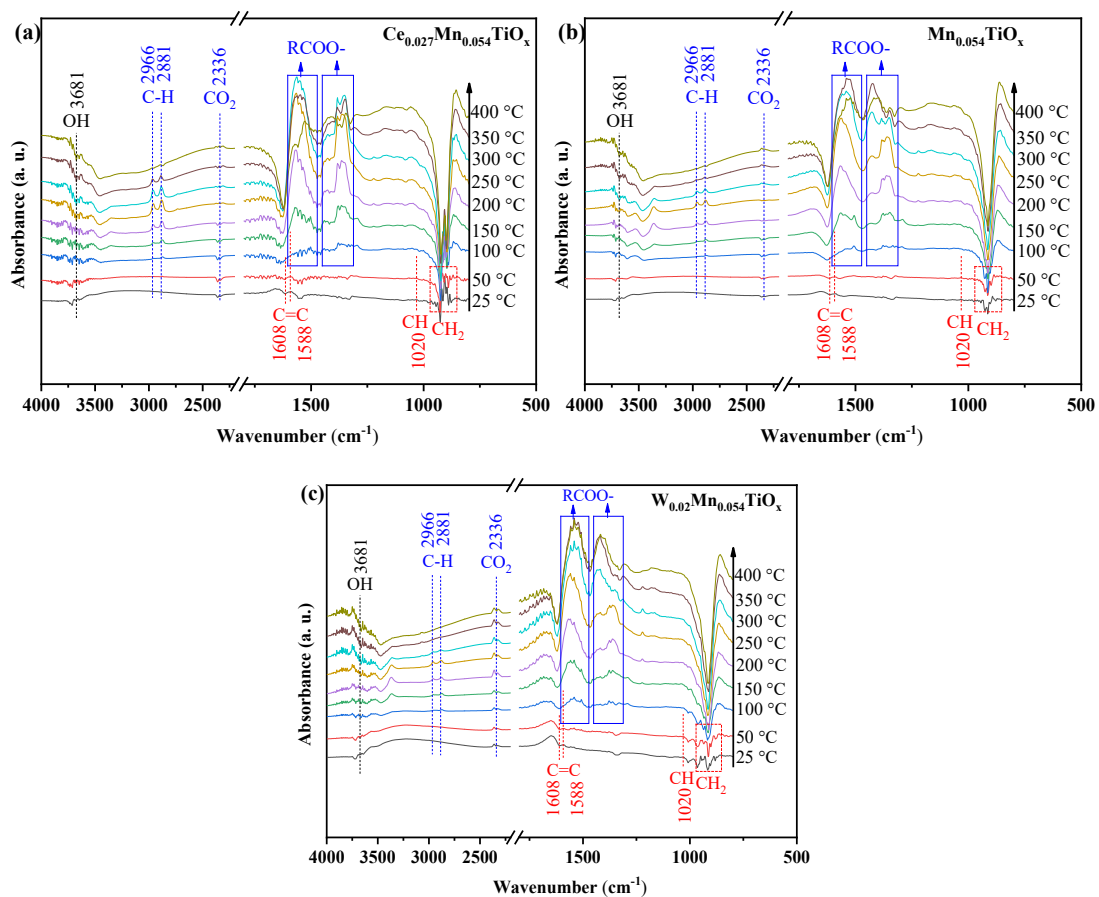


**Fig. S7.** In-situ DRIFTS spectra of 1,3-BD oxidation over  $\text{Ce}_{0.027}\text{Mn}_{0.054}\text{TiO}_x$ ,  $\text{Mn}_{0.054}\text{TiO}_x$  and  $\text{W}_{0.02}\text{Mn}_{0.054}\text{TiO}_x$  at different reaction temperature.

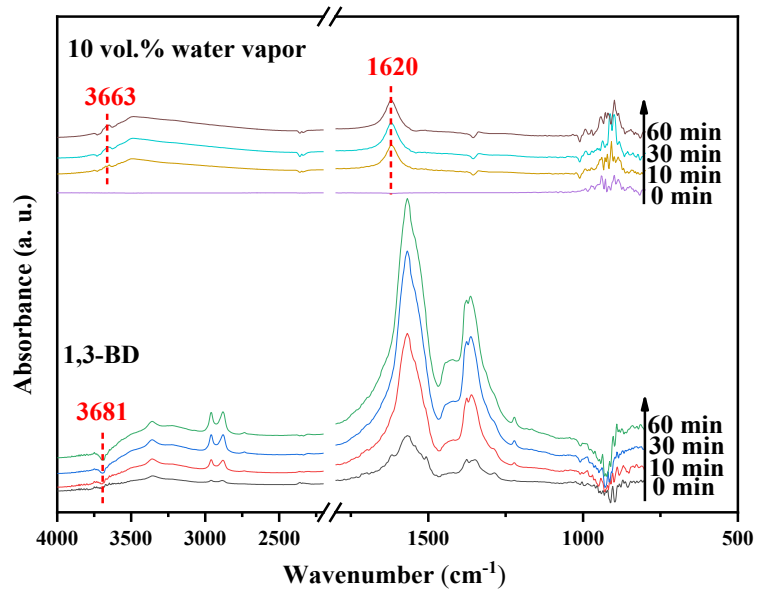


**Fig. S8.** In situ DRIFT spectra of the  $\text{Ce}_{0.027}\text{W}_{0.02}\text{Mn}_{0.054}\text{TiO}_x/1,3\text{-BD}$  and  $\text{Ce}_{0.027}\text{W}_{0.02}\text{Mn}_{0.054}\text{TiO}_x/10 \text{ vol.}\% \text{ water vapor}$  reaction systems.

**Table S1.** Variation in the mass proportion of Ce, W, Mn and Ti with the increase of the solution pH during the preparation of  $\text{Ce}_{0.027}\text{W}_{0.02}\text{Mn}_{0.054}\text{TiO}_x$  precursor by two-stage precipitation approach.

pH	Ce(%)	W(%)	Mn(%)	Ti(%)
0.8	0.38	0.77	0.11	16.43
1.5	1.42	2.23	0.12	47.01
2	1.38	1.70	0.07	47.59
5	2.78	3.54	0.08	50.47
6	4.40	3.24	1.50	37.45
7	7.47	3.72	2.66	44.96